Available online at www.sciencedirect.com
ScienceDirect
Journal of Catalysis 245 (2007) 11–24
JOURNAL OF CATALYSIS
www.elsevier.com/locate/jcat

Gas-phase carbonylation of methanol to dimethyl carbonate on chloride-free Cu-precipitated zeolite Y at normal pressure

M. Richter [a,*], M.J.G. Fait [a], R. Eckelt [a], M. Schneider [a], J. Radnik [a], D. Heidemann [b], R. Fricke [a]

[a] *Leibniz Institute for Catalysis at the University of Rostock, Branch Berlin (former ACA), P.O. Box 96 11 56, D-12474 Berlin, Germany*
[b] *Humboldt University Berlin, Faculty of Mathematics and Natural Sciences I, Department of Chemistry, Brook Taylor Str. 2, D-12489 Berlin, Germany*

Received 1 March 2006; revised 9 August 2006; accepted 8 September 2006

Available online 18 October 2006

Abstract

Chloride-free Cu/zeolite Y catalysts with Cu loading of 2–14% were prepared by precipitation from aqueous copper(II) acetate solutions and inert activation with an Ar flow at 700–750 °C for 15 h. This inert activation resulted in a considerable activity of the catalyst for the oxidative carbonylation of methanol (MeOH) to dimethyl carbonate (DMC) under normal pressure at 140–160 °C at 10–12 wt% Cu loading. Space-time yields (STY) of DMC up to 100 $g_{DMC}\, l_{Cat}^{-1}\, h^{-1}$ were achieved with a feed composed of 36% MeOH, 48% CO, 6% O_2, and balance He at a gaseous hourly space velocity (GHSV) of 3000 h^{-1}. A threshold of copper loading (5–6 wt%) was found to exist before catalysts became active. This is associated with the preferential location of copper at ion-exchange positions of the zeolite structure Y not accessible for the reactants. After saturation of these sites, the placement of copper ions within the supercage led to active catalysts. Characterization of samples at various stages of preparation by N_2 adsorption, XRD, XPS, ESR, ^{27}Al-MAS-NMR, and TPR analysis revealed that the solid-state ion exchange during inert activation is accompanied by reduction of Cu^{2+} to Cu^{+}. Copper ions exert a stabilizing effect on the crystallinity of the zeolite (in situ XRD, ^{27}Al-MAS-NMR). No crystalline metallic copper, cuprous oxide, or cupric oxide were formed (XRD), but melting occurred at 750 °C for catalysts with 14% copper loading, resulting in the formation of a glassy amorphous copper silicate/aluminate phase. The latter effect can be prevented by applying lower activation temperatures. The catalysts were prepared without using chloride, and the reaction did not require co-feeding of HCl for maintaining activity, as is needed for CuCl/zeolite catalyst formulations.

Keywords: Gas-phase carbonylation; MeOH; Dimethyl carbonate; Copper faujasite; Chloride-free

1. Introduction

Dimethyl carbonate (DMC) has increased in production volume because of its manifold applicability [1–4] as a monomer in phosgene-free polycarbonate processes, as an environmentally benign methylation agent, and as a possible gasoline-blending component due to its high oxygen content, low toxicity, and rapid biodegradability. The latter application may become attractive considering the current debate over potential groundwater contamination by the gasoline oxygenate methyl *tert*. butyl ether (MTBE).

Synthesis routes to DMC have been reviewed by Pacheco and Marshall [1] and by Delledonne et al. [2]. The conversion of MeOH by phosgene is the classic but obsolete route for DMC production,

$$COCl_2 + 2CH_3OH \rightarrow (CH_3O)_2CO + 2HCl. \quad (1)$$

A phosgene-free route is the two-stage process via methylnitrite [5],

$$2CH_3OH + 2NO + (1/2)O_2 \rightarrow 2CH_3ONO + H_2O \quad (2)$$

and

$$2CH_3ONO + CO \rightarrow (CH_3O)_2CO + 2NO. \quad (3)$$

This process runs in either a continuous or a batch mode over a $PdCl_2/FeCl_3$ co-impregnated activated carbon (AC) catalyst. A major disadvantage is the loss of chloride in form of HCl, requiring regeneration steps and co-feeding of HCl.

* Corresponding author. Fax: +49 30 6392 4392.
E-mail address: m.richter@catalysis.de (M. Richter).
URL: http://www.catalysis.de.

0021-9517/$ – see front matter
doi:10.1016/j.jcat.2006.09.009

Alternatively, the direct oxidative carbonylation of MeOH,

$$2CH_3OH + CO + (1/2)O_2 \rightarrow (CH_3O)_2CO + H_2O, \quad (4)$$

over a CuCl/zeolite catalyst is commercialized by ENICHEM in a slurry phase process [1]. But again, loss of chloride is a drawback, causing corrosion and decrement of activity. Moreover, chlorinated byproducts may affect product quality.

Several attempts have been reported for grafting Cu^+ ions, which are considered the active species on suitable supports [6–11], for a continuous gas-phase process of DMC production. In 1996, King [6,7] reported a catalyst preparation route by solid-state ion exchange (SSIE) of Cu(I) into zeolite Y starting from a physical mixture of CuCl or Cu_2O and zeolite Y. The maximum STY of DMC during continuous oxidative gas-phase carbonylation of MeOH over 24% CuCl/zeolite HY after SSIE amounted to ca. 40 $g_{DMC}\, l_{Cat}^{-1}\, h^{-1}$ at 130 °C (GHSV, 829 h^{-1}). Using Cu_2O for SSIE resulted in less active catalysts with rapid deactivation during time on stream, and a sample made by liquid-phase ion exchange with $Cu(NO_3)_2$ solution had no activity at all under the reaction conditions applied.

Other proposals to get active and stable catalysts for this gas-phase process are numerous but do not convincingly improve the STY of DMC. Anderson and Root [8,9] used zeolites 13X and ZSM-5 to anchor Cu cations by SSIE starting with a physical mixture of CuCl and the zeolite. A CuCl catalyst heterogenized on diamide-immobilized copper on SBA-15 was reported by Cao et al. [10], and $CuCl_2$ immobilized on amino-functionalized MCM-41 and MCM-48 mesoporous structures was used by Yang et al. [12]. Drake et al. [11] proposed Cu/SiO_2 prepared by precursor grafting (using Cu alkoxides) or chemical vapor deposition (using CuCl) as a catalyst for DMC production through gas-phase oxidative carbonylation of MeOH. Yang et al. [12] proposed a $PdCl_2$–$CuCl_2$–CH_3COOK co-impregnated AC catalyst for the gas-phase oxidative carbonylation of MeOH with considerable STY of DMC (ca. 390 $g_{DMC}\, l_{Cat}^{-1}\, h^{-1}$). However, the catalyst suffered considerable deactivation already after a process time of 6 h. Obviously, chloride is essentially needed for stabilization of active copper sites. Preparation routes using other copper compounds (Cu_2O, $Cu(NO_3)_2$) did not lead to active catalysts.

Here we report a catalyst preparation route that does not use any halogenide but nevertheless leads to catalysts with appreciably high and stable STY of DMC under continuous-flow conditions at normal pressure. The principal novelty of the approach involves the use of copper(II) salt solutions (although Cu^+ is finally required for catalysis) for preparation of a precursor that is activated by autoreduction of Cu^{2+} to Cu^+ under inert conditions at elevated temperatures. The preparation is accomplished by removal of residual Brønsted acid sites, thus tuning the redox system Cu^{2+}/Cu^+.

The route applied for preparing appropriate precursors consists of precipitating copper hydroxide in the presence of NH_4-Y powder suspended in distilled water. The copper content was varied over a range of 2–14 wt%. Interpretation of the catalytic results is based on characterization data from N_2 adsorption measurements, XRD (in situ as well as ex situ), XPS, ESR, ^{27}Al-MAS-NMR spectroscopy, and temperature-programmed reduction (TPR).

2. Experimental

2.1. Catalyst preparation

Preparation started with a commercial zeolite Y in its NH_4 form (Aldrich, Germany). For precipitation of $Cu(OH)_2$, a specified amount of dried NH_4-Y powder was suspended in distilled water and, in quick succession, a $Cu(CH_3COO)_2$ solution (0.1 M) and a tetramethyl ammonium hydroxide solution (10 wt%, pH = 13) were added. Thus, contact of the NH_4-Y zeolite and $Cu(CH_3COO)_2$ solution for a longer time is avoided, to minimize ion exchange at the acidic conditions (pH ≈ 4). The use of inorganic strong bases for pH increase is not possible because of competitive exchange of Na^+ (in the case of NaOH) or K^+ (in the case of KOH) into the zeolite. Adding ammonium hydroxide solution would lead to formation of stable copper tetraammine complexes and prevent precipitation. $Cu(OH)_2$ precipitated after addition of the organic base up to pH values of 8–9. Subsequent heating of the slurry to 80 °C caused a color change from blue to brown, indicating conversion of $Cu(OH)_2$ to dispersed CuO. Afterward, the slurry was filtered, washed with distilled water three times, and dried at 120 °C overnight. There was no copper in the residual solution, so the copper content of the samples corresponded to the copper concentration of the acetate solution.

Samples are denoted as "synthesis forms" at this stage. After calcination at 400 °C in static air for 2 h, the catalysts are denoted as "precursors," because all samples at this stage have only marginal activity for the carbonylation reaction.

The activation was carried out by conducting an argon stream (50 $cm^3\, min^{-1}$) through the catalyst bed at 700–750 °C for 15 h. The highest temperature required for activation depends on the Cu loading. In a first series, the activation temperature was kept constant at 750 °C (standard). A second series applied lower activation temperatures for selected samples with high Cu loading.

Samples are designated as xxCu-Y_{zzz} with the copper content xx in front (in wt%) and the pretreatment or activation temperature zzz as subscript of the zeolite (in °C). The "synthesis" form (drying of the sample at 120 °C overnight), the "precursor" (calcination at 400 °C in air for 2 h or 24 h), and the "activated" form (inert dry treatment under flow conditions at 700–750 °C for 15 h) are differentiated. The overall exchange capacity of the parent zeolite Y was determined by decomposition of the ammonium form (see Section 2.2). Sample data are summarized in Table 1.

2.2. Characterization

Surface areas and pore volumes were determined from nitrogen adsorption isotherms at 77 K using the ASAP 2010M characterization unit (Micromeritics). Samples were outgassed at 400 °C for 2 h under vacuum; the surface area was calculated

Table 1
Sample characteristics

Precursor	S_{BET} ($m^2\,g^{-1}$)	V_P ($cm^3\,g^{-1}$)	Catalyst	S_{BET} ($m^2\,g^{-1}$)	V_P ($cm^3\,g^{-1}$)
NH_4-Y_{120}	927	0.35	NH_4-Y_{750}	133	0.06
2Cu-Y_{400}	856	0.33	2Cu-Y_{750}	543	0.21
4Cu-Y_{400}	796	0.31	4Cu-Y_{750}	778	0.31
6Cu-Y_{400}	n.d.[a]	n.d.	6Cu-Y_{750}	597	0.24
8Cu-Y_{400}	n.d.	n.d.	8Cu-Y_{750}	564	0.23
10Cu-Y_{400}	734	0.29	10Cu-Y_{750}	576	0.23
			10Cu-Y_{725}	635	0.26
			10Cu-Y_{700}	680	0.27
12Cu-Y_{400}	702	0.28	12Cu-Y_{750}	266	0.11
			12Cu-Y_{725}	600	0.24
			12Cu-Y_{700}	609	0.24
14Cu-Y_{400}	719	0.28	14Cu-Y_{750}	2	0.00

[a] n.d.—not determined.

using the BET equation. Values used throughout the paper are not corrected for the percentage of copper.

Temperature-programmed decomposition of the ammonium zeolite form was performed in a He flow (flow rate, 30 $cm^3\,min^{-1}$) heating 0.3 g of NH_4-Y with a rate of 10 K min^{-1} up to 600 °C and maintaining the sample isothermally at this temperature until the ammonia concentration reached the baseline. The ammonia gas-phase concentration was recorded continuously by a thermal conductivity detector (TCD). Before detection, the gas flow was conducted through a KOH trap to remove desorbed water. The concentration of Brønsted acid sites was calculated on the basis of the desorbed ammonia. In addition, desorbed ammonia was conducted through 0.05 N H_2SO_4 and back-titrated with 0.05 N NaOH after completion of the run.

TPR measurements were performed applying an AMI-100 catalyst characterization system (Zeton/Altamira) equipped with a TCD for monitoring the H_2 consumption from a feed stream containing 5 vol% H_2 in Ar. TPR was started at 50 °C with a heating rate of 10 K min^{-1}. One TPR run was carried out with the precursor sample 10Cu-Y_{400} (sample weight, 0.06 g) without further pretreatment up to a maximum temperature of 800 °C. A second TPR run was taken from a fresh precursor sample after inert in situ activation at 750 °C with dry argon flow for 10 h, and a third run was taken from a fresh sample activated according to the second run but reoxidized in situ at 500 °C with air (flow rate, 50 $cm^3\,min^{-1}$) for 1 h. Results are graphically presented in form of H_2 consumption (in arbitrary units) versus temperature, the sample weight was normalized to 0.1 g. Calibration of the peak areas of the TPR profiles was performed according to the standard routine by introducing argon pulses into the 5 vol% H_2/Ar flow. Average values from seven pulses were taken to determine the calibration factor. However, discussion is confined to qualitative features of the TPR profiles, because already the precursor sample 10Cu-Y_{400} contained small amounts of Cu^+ ions (vide XPS), and the reduction was not completed at 800 °C. These two peculiarities do not allow a clear balance of the H_2 consumption.

Ex situ X-ray diffraction measurements were carried out using a STADI P (STOE) setup with Debye-Scherrer geometry and a Ge primary monochromator with Cu$K\alpha$1 radiation. The XRD patterns were scanned in the 2θ range of 6°–60° (step width, 0.5°; 100 s per step) and recorded with a position-sensitive detector (PSD). Data interpretation was carried out using the WinXpow software (STOE) and the Powder Diffraction File database of the International Centre of Diffraction Data (ICDD). A Theta/Theta diffractometer (Seifert/FPM) with a Bühler HDKS1 heating chamber was used for the temperature-programmed in situ investigations.

In situ X-ray powder patterns were scanned with Cu$K\alpha$ radiation at normal atmosphere in a temperature range of 150–850 °C. The patterns were recorded in Bragg–Brentano geometry with a scintillation counter.

The XPS data were recorded with a VG ESCALAB 220iXL unit using Al$K\alpha$ radiation ($E = 1486.6$ eV) at a base pressure of the UHV chamber of ca. 1×10^{-7} Pa. The spectra were referenced to the Si_{2p} peak of SiO_2 at 103.3 eV. Peak position and area were determined after satellite and background subtraction and fitting with Gaussian–Lorentzian curves. The amount of a component and thus the composition of the near-surface region was determined from the peak area after division by the element-specific Scofield factor and the analyzer-specific transmission function.

ESR spectra were recorded on a Bruker ELEXSYS 500-10/12 spectrometer in X-band (about 9.5 GHz) at 293 K (room temperature) and 77 K (liquid nitrogen temperature) after in situ evacuation at room temperature for 1 h. The magnetic field was measured with respect to a DPPH standard.

Solid-state ^{27}Al-MAS-NMR spectroscopy was carried out on a Bruker AVANCE 400 spectrometer at 104.27 MHz. The ^{27}Al-MAS-NMR spectra were obtained at a spinning speed of 12 kHz using a Bruker 4-mm MAS probe. All experiments were performed using single-pulse excitation with a pulse width of 1 µs ($\pi/6$-pulse) and an accumulation of 128 scans with a relaxation delay of 5 s. The isotropic chemical shifts, reported in ppm, are relative to an external sample of 1.0 M $AlCl_3$.

2.3. Catalytic measurements

Catalytic measurements were performed in a parallel 16 channel flow microreactor system (Fig. 1) at normal pressure with a feed composed of 36% MeOH, 48% CO, 6% O_2, 1% Ar (internal standard), and balance He. The GHSV amounted to 3000 h^{-1}. MeOH was fed into the main stream by a syringe via an evaporator. Analysis was carried out by an on-line coupled HP GCD system G18000 C (Agilent Technologies). Separation of the MeOH, dimethylether (DME), methylformate (MF), dimethoxymethane (DMM), and DMC components was achieved on a capillary column (HP-5MS, 30 m × 0.25 mm × 25 µm, split 25:1, carrier He) at 40 °C. Detection was performed by MS working in the single-ion mode (SIM) using $m/e = 45$ for identification.

MeOH conversion (X_{MeOH}) was calculated from the product balance taking into account the formation of DMC, DMM, DME, MF (neither formaldehyde, formic acid, or any further

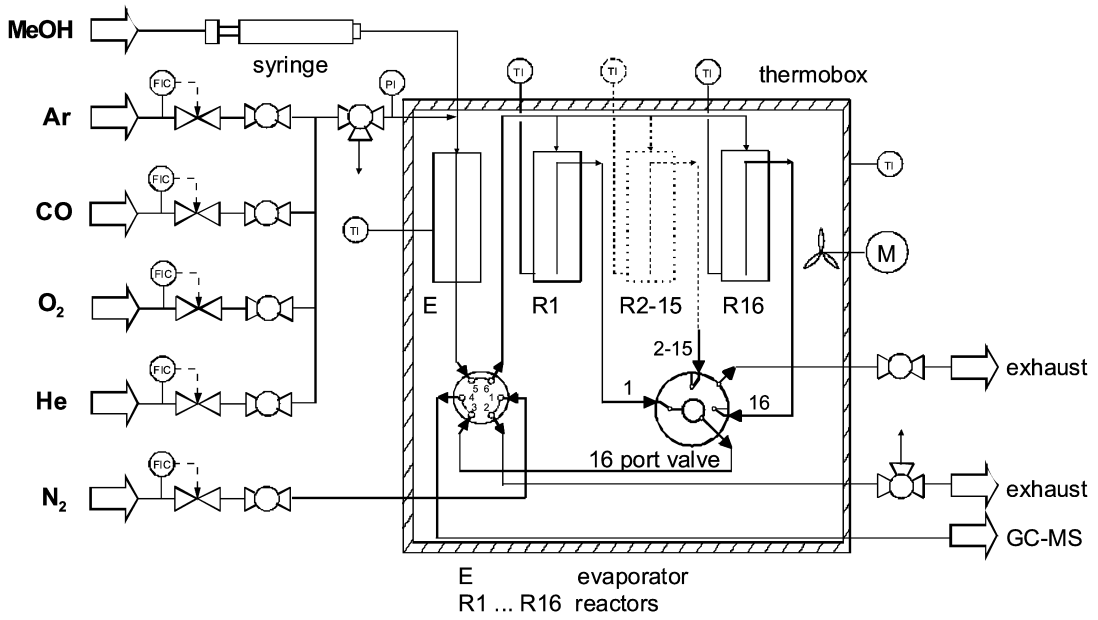

Fig. 1. Experimental setup for oxidative carbonylation of MeOH at normal pressure.

C-containing products were detected), according to the stoichiometry of the following reactions:

$$3CH_3OH + (1/2)O_2 \rightarrow (CH_3O)_2CH_2 + 2H_2O \quad \text{(DMM)}, \quad (5)$$

$$2CH_3OH \rightarrow (CH_3)_2O + H_2O \quad \text{(DME)}, \quad (6)$$

and

$$2CH_3OH + O_2 \rightarrow HCOOCH_3 + 2H_2O \quad \text{(MF)}. \quad (7)$$

The product selectivities were calculated referring the particular product concentration at the reactor outlet to the percentage of MeOH converted, and the STY of DMC is given as grams of DMC per liter of catalyst per hour ($g_{DMC}\, l_{Cat}^{-1}\, h^{-1}$).

3. Results

3.1. Characterization

3.1.1. N_2 adsorption measurements

BET surface areas (S_{BET}) of the precursors (not corrected for the Cu loading) indicate a systematic decrease from 927 $m^2\, g^{-1}$ (NH_4-Y_{120}) to 719 $m^2\, g^{-1}$ for 14Cu-Y_{400} (Table 1). Activation at standard temperature (750 °C) resulted in a further loss of surface area, depending on the Cu loading. The Cu-free NH_4-Y zeolite was nearly completely destroyed at 750 °C; the surface area was as low as 133 $m^2\, g^{-1}$. Surprisingly, copper loading of only 2 wt% maintained a surface area of 543 $m^2\, g^{-1}$ after activation (sample 2Cu-Y_{750}, cf. Table 1), and at higher Cu loading (up to 10 wt%), the resulting surface areas had an average loss of about 20% after activation at 750 °C compared with the corresponding precursors. However, copper loadings >10 wt% led to a dramatic decrease in surface area, reaching 2 $m^2\, g^{-1}$ at 14 wt% Cu. A dense phase was formed, characterized by a dark-brown color (intact samples are blue-green after activation). Pore volumes showed the same patterns, because they were derived from the same experimental N_2 uptake curves. Maximum pore volumes amounted to 0.35 $cm^3\, g^{-1}$, whereas the dense phase had practically no pore volume at all.

Further data included in Table 1 for samples with 10 and 12 wt% Cu loading demonstrate that a higher surface area was retained when an activation temperature below 750 °C was chosen. This is particularly apparent for samples 12Cu-Y_{750} and 12Cu-Y_{725}, where, after activation at 700 or 725 °C, a surface area of 609 or 600 $m^2\, g^{-1}$ was found, respectively, compared with only 266 $m^2\, g^{-1}$ after activation at 750 °C. Thermoanalytical investigation of sample 12 Cu-Y_{400} (not shown) found a weak exothermic peak between 725 and 750 °C. Taking into account that the thermoanalytical measurement was relatively fast (temperature ramp 10 $K\, min^{-1}$ vs 15 h of isothermal standard activation treatment), this exothermic peak is taken as indicating the start of thermal breakdown of the zeolite structure.

This underlines the fact that a balance must be found between the Cu loading and the appropriate activation temperature. In fact, the thermal stability of the modified Y zeolite depends on the Cu loading. Up to 10 wt%, the highest activation temperature possible (leaving the zeolite structure intact) was near 750 °C. Further enhancement of the Cu content restricted the maximum temperature of activation as formation of the dense copper silicate phase was accompanied by destruction of the zeolite structure.

N_2 adsorption isotherms are of type I, characteristic for microporous zeolites. The type of isotherm is preserved during the preparation steps (precursor and activated sample) with no indication of mesoporosity, as shown for samples NH_4-Y_{400}, 10Cu-Y_{400}, and 10Cu-Y_{750} in Fig. 2.

3.1.2. Temperature-programmed conversion of NH_4-Y to H-Y

Fig. 3 shows the profile of NH_3 release from the parent NH_4-Y zeolite during temperature-programmed inert heating. NH_3 release occurred between 200 and 500 °C with a maximum centered at 278 °C and a shoulder located around 385 °C.

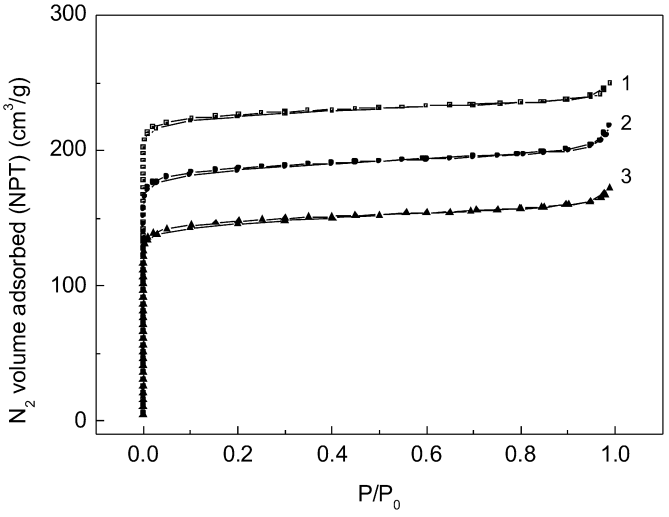

Fig. 2. N_2 adsorption isotherms for (1) NH_4-Y_{400} (■), (2) precursor 10Cu-Y_{400} (●), and (3) activated sample 10Cu-Y_{750} (▲).

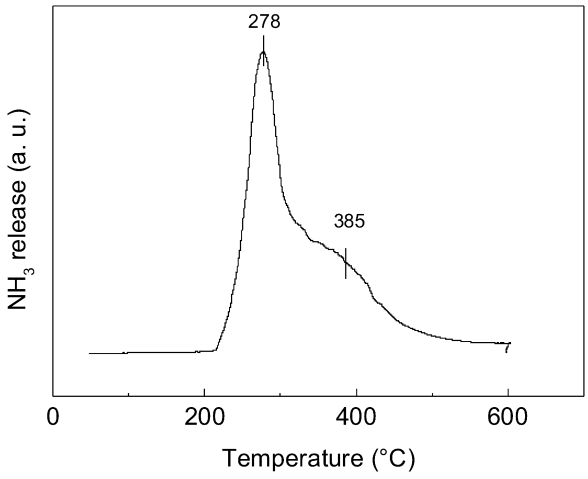

Fig. 3. Profile of NH_3 release (arbitrary units) from NH_4-Y during temperature-programmed inert heating. Heating rate 5 K min^{-1}, sample weight 0.3 g, 30 cm^3 min^{-1} He flow.

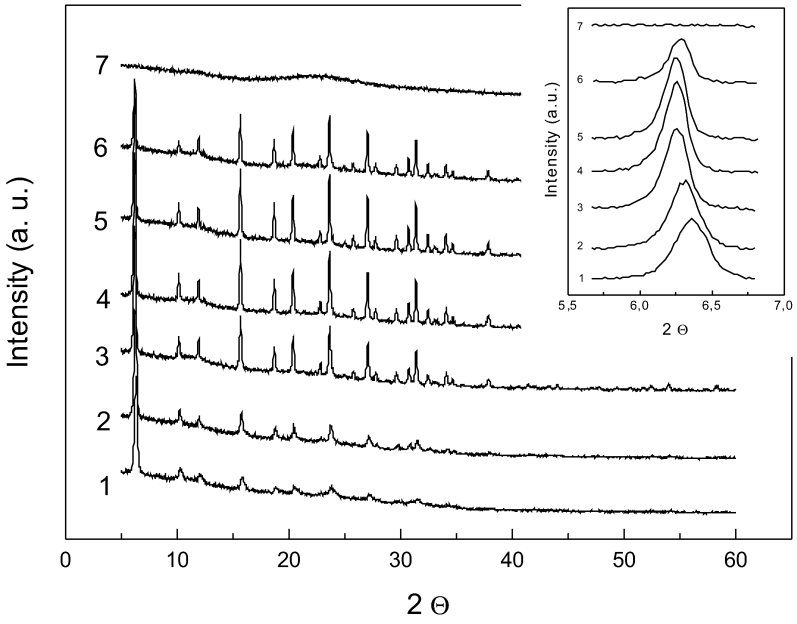

Fig. 4. XRD patterns of samples 2Cu-Y_{750} (1), 4Cu-Y_{750} (2), 6Cu-Y_{750} (3), 8Cu-Y_{750} (4), 10Cu-Y_{750} (5), 12Cu-Y_{750} (6), and 14Cu-Y_{750} (7). The inset shows a zoomed view of the 2θ range 5.5°–7°.

The overall concentration of Brønsted acid sites amounted to 2.62 mmol g^{-1}. This is equivalent to the exchange capacity of the zeolite and allowed fixation of 2.62 mmol g^{-1} Cu^+ (16.7 wt% Cu) or 1.31 mmol g^{-1} Cu^{2+} (8.4 wt%), assuming strict electroneutrality.

3.1.3. X-ray diffraction

X-ray diffraction patterns of the activated catalyst samples (2–14 wt% Cu) are shown in Fig. 4. All diffraction lines are attributable to the zeolite structure Y. The samples contain neither crystalline copper oxides nor metallic copper. It can be seen that the intensity of zeolite diffraction lines was low for samples 2Cu-Y_{750} and 4Cu-Y_{750} but increased for samples 6Cu-Y_{750}, 8Cu-Y_{750}, and 10Cu-Y_{750}. Decreased intensity is observed for 12Cu-Y_{750}. A breakdown of the zeolite structure occurred during activation of sample 14Cu-Y_{400}, but without formation of any crystalline Cu-containing phase.

Two features of the XRD patterns need to be explained: (i) the increased intensity of zeolitic diffraction lines associated with a smaller full width at half maximum (FWHM) of the peaks, and (ii) the shift of the diffraction lines to lower 2θ values with increasing copper content (cf. inset to Fig. 4).

Changes in intensity are associated with the degree of crystallinity, whereas FWHM reflects variations in particle size. Qualitatively, it can be concluded that the crystallinity of the zeolite was poor for samples 2Cu-Y_{750} and 4Cu-Y_{750} but improved with higher Cu loading up to 10 wt% (sample 10Cu-Y_{750}). Crystallinity of sample 12Cu-Y_{750} deteriorated, and melting of the precursor 14Cu-Y_{400} during the activation procedure destroyed the zeolite structure completely. This conclusion

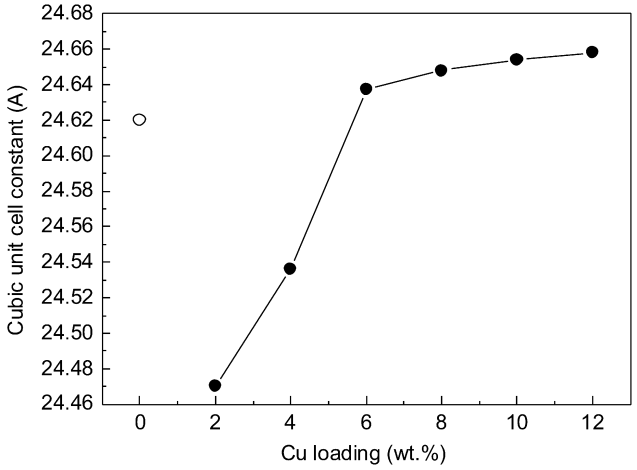

Fig. 5. Unit cell dimension of zeolite Y in dependence on Cu loading. (○) NH_4-Y_{400} from in situ XRD (cf. Fig. 6).

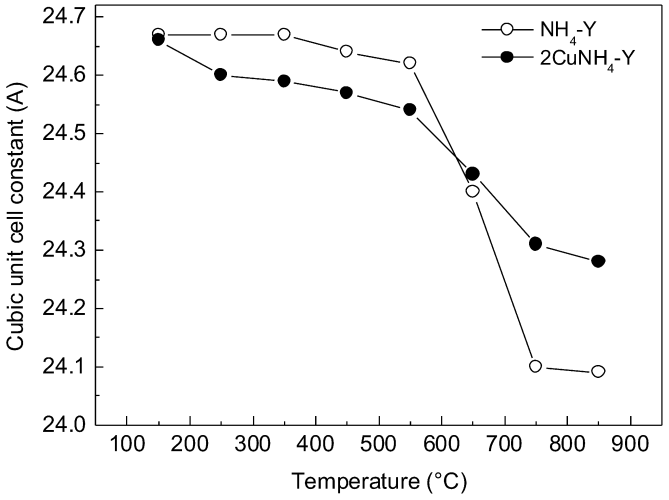

Fig. 6. In situ XRD. Unit cell constant of NH_4-Y_{120} (○) and sample 2Cu-Y_{120} (●) vs temperature under ambient air.

is supported by the observed dependence of the surface area on the Cu loading for the activated samples (cf. Table 1). Intact crystallinity of the zeolite is characterized by high surface area and pore volume. The up and down of the crystallinity versus Cu loading as documented by XRD measurements for the activated samples is fairly reflected by the surface areas/pore volumes.

Smaller FWHM values correspond to larger crystallite sizes. Whether larger crystallites were built during the preparation process is not clear. But the variation of the FWHM of diffraction peaks paralleled the changes in intensity of the diffraction lines and obviously was associated with the modification of zeolite crystallinity, as discussed earlier. Altogether, it is evident that introduction of copper into the zeolite enhanced the resistance against thermal deterioration up to a borderline value that depends on the Cu loading and the activation temperature.

The shift in 2θ values indicates characteristic changes of unit cell parameters of the zeolite Y depending on the copper content of the activated samples (Fig. 4, inset). A detailed view is shown in Fig. 5. Zeolite NH_4-Y (unit cell composition $(NH_4)_{58}[Al_{58}Si_{134}O_{384}]\cdot 240H_2O$) crystallizes in a cubic space group with the lattice constant $a = 24.645$ Å [13]. The Cu-free sample NH_4-Y_{400} revealed a cell constant of 24.62 Å. After thermal pretreatment of the ammonium form at 400 °C (to simulate the precursor state), the zeolite was in a mixed NH_4-H form, and the unit cell size was correspondingly lower. A contraction of unit cell size is known to occur during transition from NH_4-Y to H-Y [14]. The zeolite unit cell size was increased with increasing Cu loading (activated samples). A nearly linear increase can be seen for samples 2Cu-Y_{750}, 4Cu-Y_{750}, and 6Cu-Y_{750}, whereas for samples 6Cu-Y_{750}, 8Cu-Y_{750}, 10Cu-Y_{750}, and 12Cu-Y_{750}, the unit cell size of the zeolite increased only marginally.

Subjecting zeolite NH_4-Y_{120} a stepwise temperature increase by 100 K from 150 to 850 °C clearly confirms that replacement of NH_4^+ ions by H^+ during the thermal decomposition of NH_4^+ within the temperature range from 300 to 550 °C (cf. Fig. 3) was accompanied by a unit cell contraction (Fig. 6). Further temperature increase above 600 °C initiated a strong decrease in the unit cell dimension that might be attributed to the thermal dehydroxylation of Brønsted acid sites with formation of Lewis acid sites. But simultaneously, the crystallinity of the zeolite was destroyed, as followed from the low BET surface area of the Cu-free NH_4-Y_{120} zeolite after "activation" at 750 °C (cf. Table 1).

Sample 2Cu-Y_{120} had nearly the same unit cell dimension as the NH_4-Y_{120} zeolite at 150 °C ($a = 24.66$ Å vs $a = 24.67$ Å). During further heating, replacement of NH_4^+ ions (ion radius 1.43 Å) by Cu^{2+} ions (radius 0.72 Å) occurred, accompanied by unit cell contraction. Reduction of Cu^{2+} to Cu^+ (ion radius 0.96 Å) was of minor importance, because an air flow was used during the measurements. At higher temperatures (650–850 °C), the unit-cell dimension of sample 2Cu-Y_{120} was larger than that of the Cu-free zeolite. Obviously, exchanged copper ions prevent further unit cell contraction.

3.1.4. ^{27}Al-MAS-NMR spectroscopy

Results of ^{27}Al-MAS-NMR spectroscopy are shown in Fig. 7. The parent NH_4-Y_{120} zeolite had practically no octahedrally coordinated Al (not shown). Calcination of NH_4-Y at 400 °C in static air (to simulate the precursor state) led to dealumination with the characteristic signal of nonframework Al at −1 ppm. However, the preponderant part of the Al was on tetrahedrally coordinated framework positions (signal at 60 ppm). Penta-coordinated Al (signal at around 30 ppm) was not present. Sample 2Cu-Y_{750} exhibited a part of nonframework Al at 2 ppm, but this low percentage was further decreased with higher Cu loading until exclusively tetrahedrally coordinated framework Al was seen at 6 wt% Cu loading (sample 6Cu-Y_{750}). This underlines the conclusions drawn from results of XRD measurements. Copper ions fixed to the zeolite framework improved the resistance of the zeolite framework against thermal deterioration. Further correspondence between results of XRD measurements and ^{27}Al-MAS-NMR spectroscopy was observed for samples 12Cu-Y_{750} and 14Cu-Y_{750}. The destruction of the zeolite was also evident from the NMR spectra,

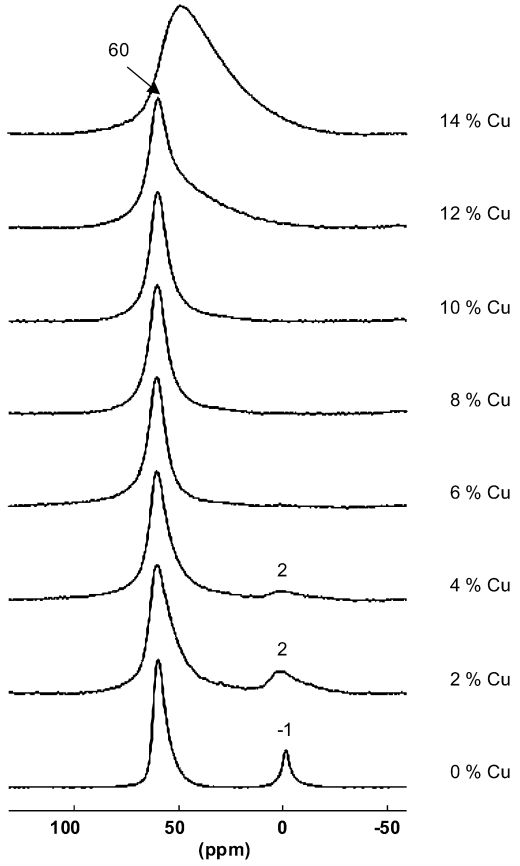

Fig. 7. ^{27}Al-MAS-NMR spectra (only the central range is displayed) of NH_4-Y_{400} zeolite and of catalyst samples 2Cu-Y_{750}, 4Cu-Y_{750}, 6Cu-Y_{750}, 8Cu-Y_{750}, 10Cu-Y_{750}, 12Cu-Y_{750}, and 14Cu-Y_{750} (from bottom to top).

because the signal of Al was asymmetrically broadened and shifted to lower values. Most significant, for sample 14Cu-Y_{750}, aluminium was in a new environment due to the amorphous phase formed (vide XRD).

3.1.5. X-ray photoelectron spectroscopy

The normalized Cu_{2p} spectra of selected samples with 2 and 10 wt% Cu loadings are shown in Figs. 8a and 8b, respectively. A typical fingerprint with four peaks in the Cu_{2p} spectrum indicating Cu^{2+} is seen for sample 10Cu-Y_{120}. The transition from Cu^{2+} to Cu^{+} species can be traced by the intensity of satellite bands and by the chemical shift of the $Cu_{2p_{3/2}}$ peak. Thus, Cu^{2+} obviously was reduced during precursor preparation and sample activation. These reduced species can clearly be identified as Cu^{+} due to the kinetic energy of the Cu LMM Auger electrons (Table 2). The energies were lower for Cu^{+} than for Cu^{0} or Cu^{2+}. Al/Si ratios, Cu^{2+}/Cu^{+} percentages, and Cu/(Al + Si) ratios in the near-surface region (the outermost 50–100 Å of the samples) are summarized in Table 3. Samples 2Cu-Y_{120} (synthesis form), 2Cu-Y_{400} (precursor), and 2Cu-Y_{750} (activated catalyst) show characteristic differences of the Cu valence states and Al/Si ratios compared with corresponding samples with 10 wt% Cu loading.

Samples 2Cu-Y_{120}, 2Cu-Y_{400} and 2Cu-Y_{750} had nearly 50, 70, and 100% Cu^{+}, respectively, whereas samples 10Cu-Y_{120}, 10Cu-Y_{400} and 10Cu-Y_{750} contained 0, 35, and 59% Cu^{+}, respectively.

The synthesis form of samples exhibited a higher Cu/(Al + Si) surface ratio than the precursors and activated catalysts, best

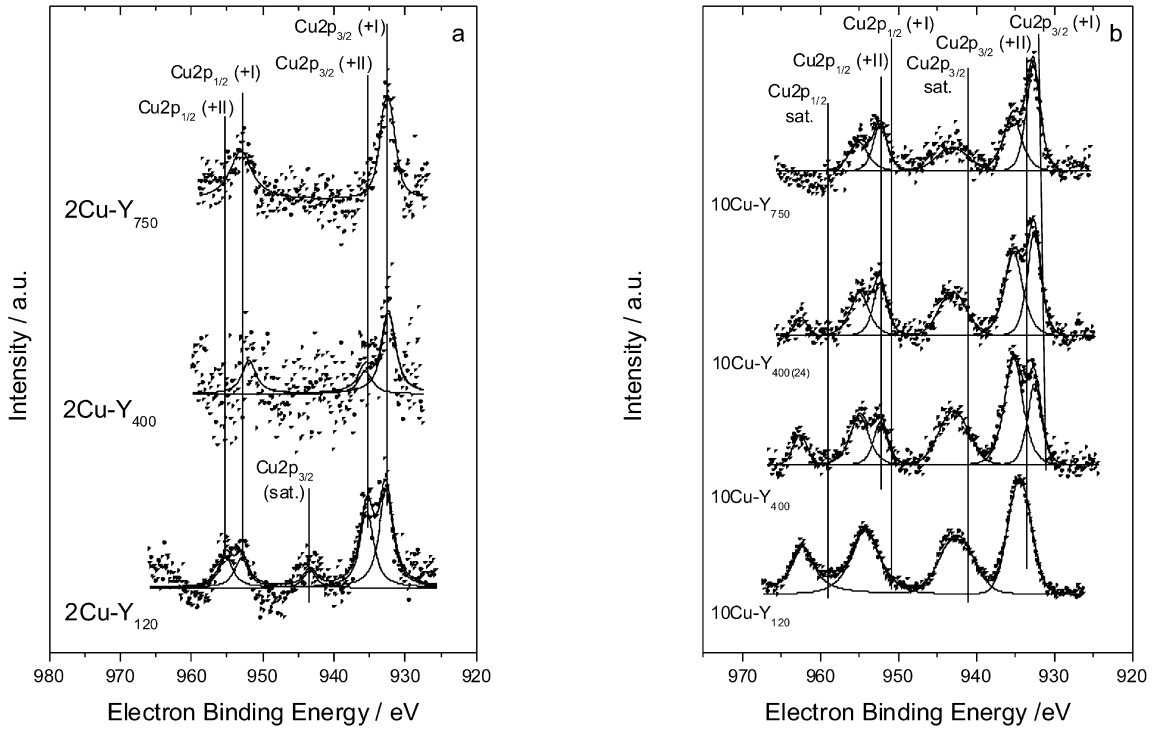

Fig. 8. XPS of samples 2Cu-Y_{120}, 2Cu-Y_{400} and 2Cu-Y_{750} (a), and of samples 10Cu-Y_{120}, 10Cu-Y_{400}, 10Cu-$Y_{400(24)}$ and 10Cu-Y_{750} (b).

Table 2
XPS results of sample 10Cu-Y

	Electron binding energy $Cu_{2p_{3/2}}$		Kinetic energy Cu LMM (eV)
	Cu^+	Cu^{2+}	
Sample			
10Cu-Y_{120}		934.4	916.6
10Cu-$Y_{400(2)}$	932.5	935.2	914.4
10Cu-$Y_{400(24)}$	932.6	935.2	914.4
10Cu-Y_{750}	932.7	935.4	913.7
References			
Cu^0	932.7		918.6
Cu_2O	932.5		916.2
CuO	933.6		918.1

Table 3
XPS data. Al/Si ratios, percentages of Cu^{2+}/Cu^+ and overall Cu/(Al + Si) ratios

Sample	Al/Si ratio	Cu^{2+}	Cu^+	$Cu_{2p}/(Al_{2s} + Si_{2s})$
2Cu-Y_{120}	0.40	49	51	0.02
2Cu-Y_{400}	0.29	30	70	0.00
2Cu-Y_{750}	0.27	0	100	0.01
10Cu-Y_{120}	0.64	100	0	0.29
10Cu-Y_{400}	0.61	64	36	0.05
10Cu-$Y_{400(24)}$	0.54	52	48	0.05
10Cu-Y_{750}	0.58	41	59	0.03
Bulk ratio[a]	0.43			

[a] From ICP OES.

seen for 10 wt% Cu loading. Already the preparation of the precursors led to depletion of Cu from the outer surface. This effect was further pronounced for the activated sample 10Cu-Y_{750}. This means that migration and reduction of Cu^{2+} occur already during precursor preparation, but was further enhanced during the activation process.

The presence of Cu^+ in sample 2Cu-Y_{120} is explained by a shift of the surface equilibrium between Cu^{2+} and Cu^+ in the presence of a high proton concentration with preferential stabilization of Cu^+ [15],

$$[CuOH]^+ + H^+ + e^- \leftrightarrow Cu^+ + H_2O. \quad (8)$$

The presence of Cu^+ in the precursor samples despite the oxidative treatment may be due to reduction of Cu^{2+} by ammonia resulting from thermal decomposition of NH_4^+ ions of the zeolite. However, it must be noted that the UHV conditions during XPS also can initiate reduction of Cu^{2+} ions.

The Al/Si molar ratio revealed a depletion of Al on the surface (Al/Si ratio lower than the bulk ratio) for samples with 2 wt% Cu, along with enrichment of Al on the surface for the sample with 10 wt% Cu (Al/Si ratio higher than the bulk ratio). Obviously, some Al was solved during preparation by the acetate solution at low Cu content, whereas precipitation of 10 wt% Cu shielded the surface of the zeolite crystallites and prevented dealumination. Whether a gradient of Al concentration within the zeolite crystallites was present a priori is not clear.

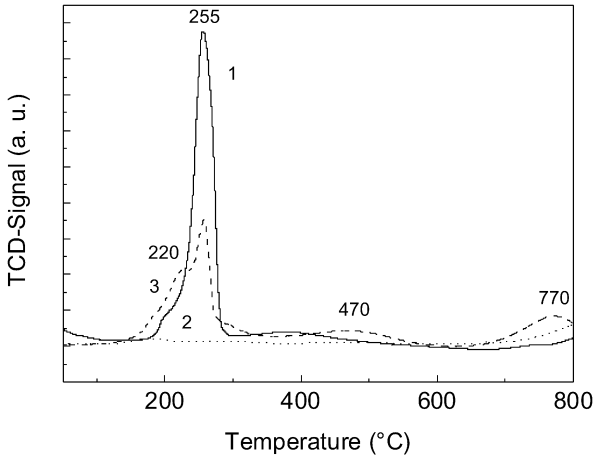

Fig. 9. TPR profile of sample 10Cu-Y_{400} (1), 10Cu-Y_{750} (activated in situ) (2), and 10Cu-Y_{750} after reoxidation in situ at 500 °C with air for 1 h (3). H_2 consumption in arbitrary units, normalized to 0.10 g sample weight.

3.1.6. TPR by H_2

For demonstration how the activation procedure affects the state of reducible copper species, the inert activation at 750 °C was followed in situ, starting with the precursor 10Cu-Y_{400}. Results are shown in Fig. 9. Reduction of sample 10Cu-Y_{400} occurred at about 180 °C and the reduction proceeds in one step centered at 255 °C. (A faint shoulder at ca. 200 °C can be distinguished on the low-temperature edge of the main peak.) After in situ inert activation of a fresh sample 10Cu-Y_{400}, no reducible species were present up to 800 °C. Inert activation of a further sample 10Cu-Y_{400} and in situ reoxidation of the activated sample restored the initial TPR profile of the precursor only partly (curve 3), because the main reduction peak at 255 °C composed a significantly lower amount of reducible species than observed for the precursor. Additional reduction peaks emerge at 220, 470, and 770 °C. The reduction onset was shifted to lower temperatures (ca. 150 °C).

The reduction of Cu^{2+} in Cu-Y zeolites occurs by a two-step mechanism [16],

$$2Cu^{2+} + H_2 \leftrightarrow 2Cu^+ + 2H^+ \quad (9)$$

and

$$2Cu^+ + H_2 \leftrightarrow 2Cu^0 + 2H^+. \quad (10)$$

The reduction of Cu^{2+} ions located at ion-exchange positions of the zeolite to Cu^+ and of dispersed bulk CuO to Cu^0 occurred in the same temperature region (200–300 °C) and was difficult to separate. Cu^+ ions were stabilized on the zeolite and reduced at distinctly higher temperatures. The ease of reduction depends on the location of the cations, in the order supercage > sodalite cage > hexagonal prism [17].

The following conclusions can be derived from the TPR profiles:

(i) The precursor sample 10Cu-Y_{400} contains Cu^{2+} whose reduction occurs between 180 and 290 °C (maximum, 255 °C). A reduction of Cu^+ to Cu^0 occurs at temperatures above 800 °C (outside the experimental temperature range).

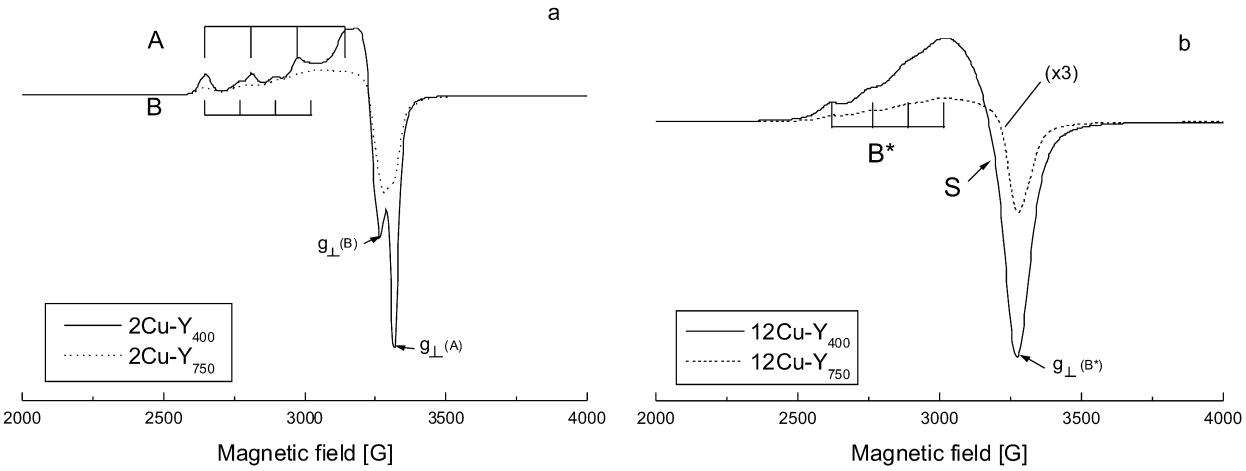

Fig. 10. ESR spectra of samples 2Cu-Y_{400} and 2Cu-Y_{750} (a), and of samples 12Cu-Y_{400} and 12Cu-Y_{750} (b) recorded at 77 K after in situ evacuation at room temperature for 1 h.

(ii) After inert thermal treatment, practically no reducible Cu^{2+} species were present, and reduction of Cu^{+} occurred outside the temperature range (onset of H_2 consumption occurred above 700 °C).

(iii) Redistribution of copper ions occurred during activation, because reoxidation cannot restore the TPR pattern of the precursor. Furthermore, not all Cu^{+} ions are reoxidized to Cu^{2+}, because the H_2 consumption centered at 770 °C indicated reduction of Cu^{+} after reoxidation. Obviously, the reducibility of Cu^{+} was now easier, because inert activation removed Brønsted acid sites through dehydroxylation, and thus reaction (10) was shifted to the right side.

3.1.7. ESR

Cu^{2+} ions are $3d^9$ paramagnetic ions that are readily observed by ESR, whereas Cu^{+} ions are diamagnetic ($3d^{10}$) and thus ESR-silent [18]. The ESR spectra of copper-loaded zeolite Y were characterized by at least two overlapping axial signals at $g_{\parallel}^{(1)} = 2.36$–$2.41$ and $g_{\parallel}^{(2)} = 2.30$–$2.34$. As such, they reflected the type of coordination of Cu^{2+} in the structure. However, the relative intensities of the two ESR signals varied with the Si/Al ratio, type of co-cation, and copper loading and were indicative of the site preference of Cu^{2+} [19]. Most authors assign the two ESR signals to Cu^{2+} ions located on different cationic sites or in different Al surroundings [20].

ESR spectra of samples 2Cu-Y_{400}, 2Cu-Y_{750}, 12Cu-Y_{400}, and 12Cu-Y_{750} are shown in Fig. 10. According to XPS, sample 2Cu-Y_{750} contained exclusively Cu^{+}, whereas ESR detected Cu^{2+}. This may be related to the different surface sensitivity of these two methods. (XPS is sensitive for the near-surface region, whereas ESR is a bulk method.) Reduction of some Cu^{2+} to Cu^{+} in the UHV under X-ray irradiation during the XPS measurements is also possible. Another reason could be the low signal-to-noise ratio of the XP spectrum of sample 2Cu-Y_{750}, which does not allow resolution of the Cu^{2+} features.

A comparison of ESR spectra (Fig. 10) from samples 2Cu-Y_{400} and 12Cu-Y_{400} shows that at only 2 wt% Cu, the hyperfine splitting (hfs) of the spectra was sufficiently resolved to obtain detailed information on the Cu^{2+} ion state. The g and hfs values are collected in Table 4. All four samples contained Cu^{2+} species in square-pyramidal or distorted octahedral coordination according to the ESR parameters [21]. In addition, after inert vacuum treatment at 500 °C, a part of Cu^{2+} was retained (not shown). However, the ESR signal intensity decreased due to reduction of Cu^{2+} to Cu^{+} or to formation of ion pairs.

Table 4
ESR parameters of samples 2Cu-Y and 12Cu-Y

Sample[a]	Signal A				Signal B			Signal B*	
	$g_{\parallel}$	$A_{\parallel}$	$g_{\perp}$	$g_{\parallel}$	$A_{\parallel}$	$g_{\perp}$	$g_{\parallel}$	$A_{\parallel}$	$g_{\perp}$
2Cu-Y_{400}	**2.328**	**166.7**	**2.038**	2.376	126.0	2.066			
2Cu-Y_{750}	2.328	166.7	2.038	**2.376**	**126.0**	**2.066**			
12Cu-Y_{400}							2.396	132.0	2.050
12Cu-Y_{750}							2.396	132.0	2.05

[a] ESR spectra were recorded at 77 K after evacuation of the samples for 1 h at room temperature; bold values indicate main signal.

A comparison of spectra for samples 2Cu-Y_{400} and 2Cu-Y_{750} (Fig. 10a) reveals changes in the ESR parameters (cf. Table 4). Whereas signal A decreased drastically in intensity, signal B increased in intensity, showing a higher $g_{\parallel}$ value and a distinctly lower hfs splitting $A_{\parallel}$. The overall intensity decreased slightly as a result of sample activation; that is, the concentration of Cu^{2+} was diminished during activation, thus confirming the autoreduction process qualitatively. According to Yu and Kevan [22] the $g_{\parallel}$ tensor at 2.33 indicates the presence of Cu^{2+} in hexagonal prisms of zeolite Y (site type I), and the $g_{\parallel}$ tensor at 2.39 was assigned to Cu^{2+} in an almost planar trigonal coordination in the six-membered ring site I′. Because site types I and I′ are close to each other and could not be occupied simultaneously [23], the change in positions could be attributed to dealumination, which was shown by ^{27}Al-MAS-NMR to proceed during activation of samples with low Cu loading. This dealumination seemed to modify the surrounding of Cu^{2+} and promote a change of position and coordination of Cu^{2+} ions.

Under the same conditions, the Cu^{2+} signal of sample 12Cu-Y_{400} was characterized by a weak hfs resolution (Table 4, sig-

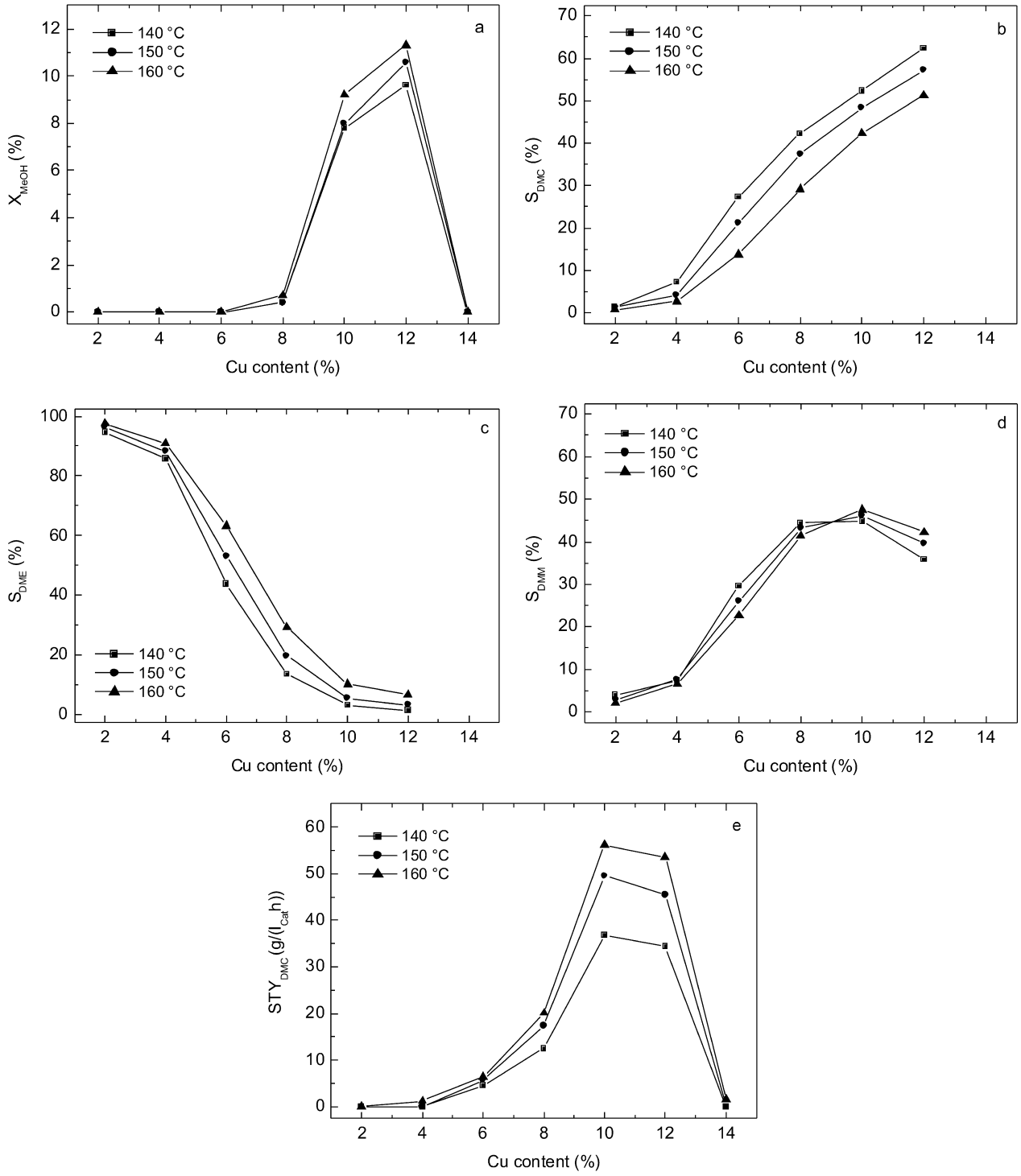

Fig. 11. Catalytic results at normal pressure, (a) MeOH conversion, (b) DMC selectivity, (c) DME selectivity, (d) DMM selectivity, (e) STY of DMC. Feed composition 36% MeOH, 48% CO, 6% O_2, 1% Ar (He balance), GHSV 3000 h^{-1}.

nal B*). The estimated parameters differed only slightly from those of signal B, possibly due to the low relative intensity of the hfs signal. The signal was overlapped by an isotropic strong signal S, which was clearly caused by interacting Cu^{2+} species (possibly Cu^{2+}–O–Cu^{2+} pairs). Sample 12Cu-Y_{750} exhibited decreased signal intensity by about one order of magnitude compared with the precursor (12Cu-Y_{400}) due to reduction of Cu^{2+} species during inert activation.

3.2. Catalysis

Conversion of MeOH, selectivities of the main products DMC, DMM, and DME, and the STY of DMC in dependence on Cu loading are shown in Figs. 11a–11e for three selected reaction temperatures: 140, 150, and 160 °C. It follows from Fig. 11a that a threshold of 6 wt% Cu loading must be passed to achieve noticeable conversion of MeOH after inert activation.

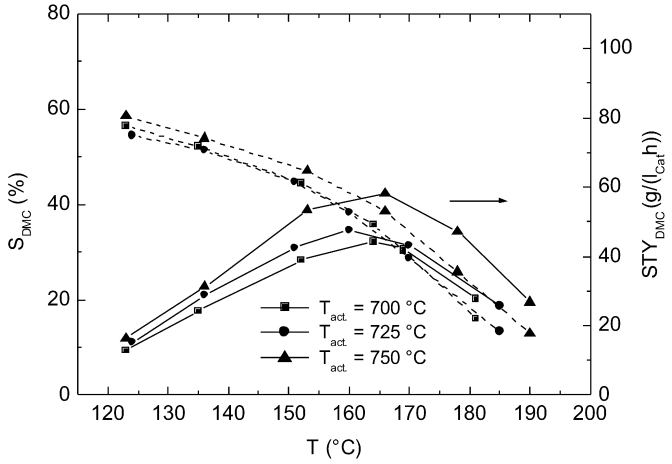

Fig. 12. Influence of activation temperature (750 °C (▲), 725 °C (●), 700 °C (■)) on the catalytic behavior of sample 10Cu-Y_{400}. DMC selectivity ((- - -), left) and STY of DMC ((—), right). Reaction conditions: feed composition 36% MeOH, 48% CO, 6% O_2, 1% Ar (He balance), GHSV 3000 h^{-1}. Normal pressure.

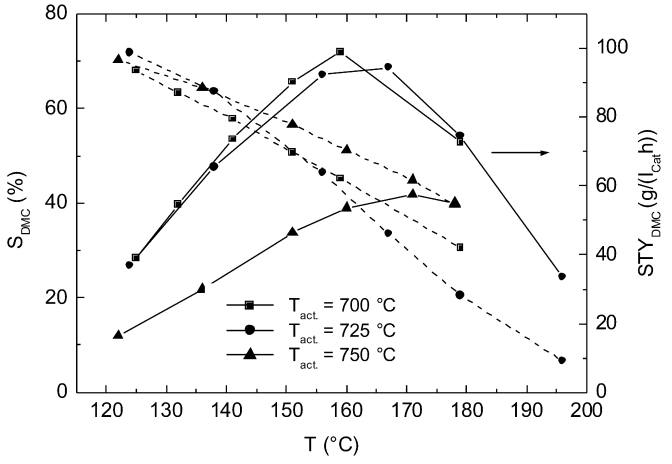

Fig. 13. Influence of activation temperature (750 °C (▲), 725 °C (●), 700 °C (■)) on the catalytic behavior of sample 12Cu-Y_{400}. DMC selectivity ((- - -), left) and STY of DMC ((—), right). Reaction conditions: feed composition 36% MeOH, 48% CO, 6% O_2, 1% Ar (He balance), GHSV 3000 h^{-1}. Normal pressure.

Maximum MeOH conversions of 9.0–11.5% were achieved at a Cu loading of 12 wt%. At a Cu loading of 14 wt% and activation at 750 °C, all activity was lost, due to the complete breakdown of the zeolite structure as shown in Sections 3.1.1 and 3.1.3.

Selectivity to DMC (Fig. 11b) monotonically increased with Cu loading and attained maximum values of 50–60% (sample 12Cu-Y_{750}) at reaction temperatures of 160 and 140 °C, respectively. This increase was mirrored by a corresponding decrease in DME selectivity (Fig. 11c). DME formed nearly exclusively over sample 2Cu-Y_{750}, but its formation was progressively suppressed at higher Cu loading, reaching values of 2–10% for sample 12Cu-Y_{750}. At a fixed Cu loading, the selectivity of DME increased with higher reaction temperature. Two possible routes of DME formation must be considered: (i) decomposition of DMC [24] and (ii) dehydration of MeOH. Anderson et al. [24] found that the decomposition of DMC was highest on H-Y but decreased with increasing Cu loading. These authors concluded that the decomposition of DMC is an acid-catalyzed reaction step. This conclusion is reconcilable with experimental findings.

The dehydration of MeOH to DME is considered of minor importance at temperatures below 200 °C according to accepted knowledge [25]. DMM selectivity passed through a maximum at a Cu loading of 10% (Fig. 11d). Space-time yields of DMC revealed a maximum value of 55 $g_{DMC}\, l_{Cat}^{-1}\, h^{-1}$ for sample 10Cu-Y_{750} at a reaction temperature of 160 °C (Fig. 11e). Formation of MF was not observed.

Based on the observation that the appropriate temperature of inert activation depended on the copper loading, the question whether the fixed activation routine at 750 °C is adequate or not was addressed for samples 10Cu-Y and 12Cu-Y. Thus, for precursors 10Cu-Y_{400} and 12Cu-Y_{400}, two lower activation temperatures—725 and 700 °C—were applied for activation. Catalytic results are presented in Figs. 13 and 14 for samples 10Cu-Y and 12Cu-Y, respectively, including results for samples 10Cu-Y_{750} and 12Cu-Y_{750} for reference. Fig. 12 shows

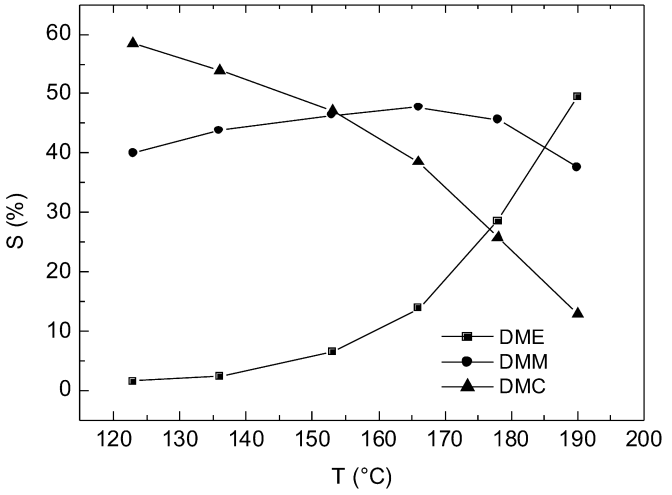

Fig. 14. Selectivities of DMC, DMM and DME vs temperature for sample 10Cu-Y_{750}. Reaction conditions: feed composition 36% MeOH, 48% CO, 6% O_2, 1% Ar (He balance), GHSV 3000 h^{-1}. Normal pressure.

that lower activation temperatures of precursor 10Cu-Y_{400} led to lower DMC selectivities and STY values.

In contrast, milder activation conditions had a beneficial effect on the performance of sample 12Cu-Y (Fig. 13). When activated at 725 or 700 °C, samples 12Cu-Y_{725} and 12Cu-Y_{700} achieved STY values of DMC of approximately 100 $g_{DMC}\, l_{Cat}^{-1}\, h^{-1}$ at 160 °C despite the slightly lower DMC selectivity.

This improvement is obviously due in part to the higher accessible surface area, 266 $m^2\, g^{-1}$ after activation at 750 °C and 609 $m^2\, g^{-1}$ after activation at 700 °C (cf. Table 1). The decreased DMC selectivity at higher temperatures is attributable to its thermal decomposition,

$$(CH_3O)_2CO \rightarrow (CH_3)_2O + CO_2. \quad (11)$$

This leads to the observed reversed pattern of DMC/DME selectivity versus reaction temperature, as shown for sample

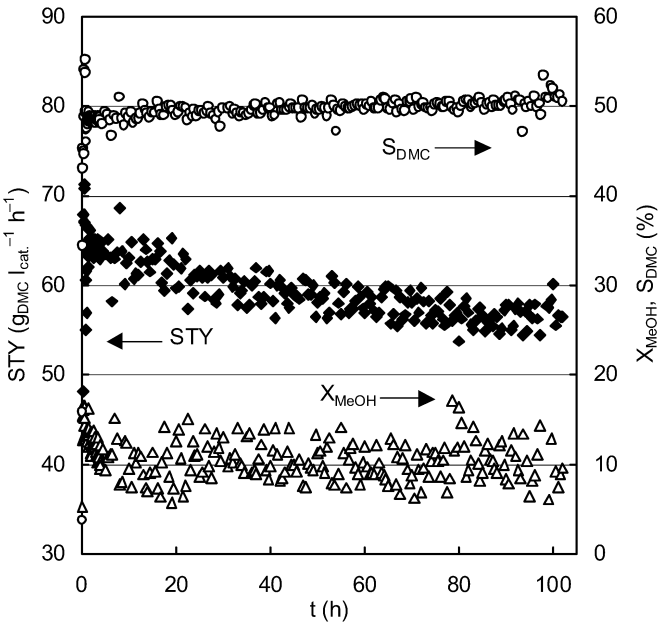

Fig. 15. Time-on stream performance of sample 10Cu-Y_{750} at 150 °C and normal pressure. Feed composition 36% MeOH, 48% CO, 6% O_2, 1% Ar (He balance), GHSV 3000 h^{-1}. STY of DMC (left), MeOH conversion X_{MeOH}, and DMC selectivity S_{MDC} (right).

10Cu-Y_{750} in Fig. 14. Dehydration of MeOH to DME, as well as total oxidation of MeOH to CO_2, played no decisive role under these conditions, especially in the temperature range chosen. An STY of ca. 60 $g_{DMC}\, l_{Cat}^{-1}\, h^{-1}$ at a reaction temperature of 150 °C could be maintained over 100 h without significant deactivation for sample 10Cu-Y_{750} (Fig. 15).

4. Discussion

The investigated catalyst series was prepared without any halogenide, starting with Cu(II) acetate solution, and forcing precipitation of dispersed Cu(II) hydroxide onto suspended NH_4-Y zeolite by enhancing the pH value through addition of a base. Catalysts showed acceptable productivity at copper contents of 10–12 wt%, provided the preparation step was completed by inert activation at an appropriate temperature, which depends on the copper loading. It turned out that a threshold of Cu loading was required to get activity for the oxidative carbonylation of methanol in the gas phase at normal pressure. The discussion that follows focuses on relevant aspects of active site formation and catalytic reaction.

4.1. Activation of the Cu-Y catalyst system

The "activation" procedure initiated a SSIE of copper ions, which become fixed to Brønsted acid sites. Replacement of acidic protons by Cu^{2+}/Cu^{+} protected the zeolite lattice against dealumination (^{27}Al-MAS NMR) and thermal deterioration (XRD, surface areas). A reduction of Cu^{2+} to Cu^{+} was already observed during preparation of the precursors and was further promoted by the final inert treatment. It is known that Cu^{2+} may be reduced during zeolite dehydration by oxide ions of water molecules, by framework hydroxyl groups [26] or by ammonia [27]. Compared with SSIE starting from a physical mixture of copper salts and zeolites, the dispersed state achieved through the precipitation technique facilitates deaggregation of copper oxide.

During inert activation, Cu^{+} is formed (the samples are grey-white). TPR (after in situ activation without intermediate influx of oxygen) of sample 10Cu-Y_{750} could not detect any further Cu^{2+} ions, but XPS (taken after intermediate storage of the activated sample at ambient atmosphere) detected nearly 40% Cu^{2+}. This proves that contact of activated samples with ambient air (containing oxygen and moisture) at room temperature leads to oxidation of Cu^{+} and formation of Cu^{2+} hydroxyl species ($[CuOH]^{+}$). These Cu^{2+} species are more easier reducible than before (shoulder at 220 °C in the TPR profile of sample 10Cu-Y_{750}, reoxidized in situ). It should be mentioned that reduction of $[Cu–O–Cu]^{2+}$ oxo-cations in zeolite ZSM-5 was reported to occur already at room temperature [29,30]. Because TPR measurements started after equilibration at 50 °C no H_2 consumption balance could be made. Therefore, the possibility that formation of $[Cu–O–Cu]^{2+}$ oxo-cations occurred at higher Cu loading could not be excluded.

After the activation procedure, the copper was finely dispersed; XRD did not reveal any crystalline copper oxide phases or metallic crystalline copper. Even the totally amorphous sample 14Cu-Y_{750} gave no reflection pattern.

Thermal dehydroxylation of Brønsted acid sites can be expected to accompany the SSIE at 700–750 °C, with formation of Lewis acidity. Lewis acid sites once formed at temperatures as high as 750 °C were not reconverted into Brønsted acid sites by adding water [28]. The concentration of protons influenced the stability of Cu^{2+}/Cu^{+} by the existing surface equilibrium [Eq. (9)]. Removing protons shifted the equilibrium to the right side, promoting Cu^{+} formation. Thus, high-temperature treatment with an O_2-purified inert gas flow actually destabilized the Cu^{2+} oxidation state by removing protons (dehydroxylation of Brønsted acid sites). This is thought to tune the redox properties of Cu^{2+}/Cu^{+}, which are preserved under reaction conditions, because rehydroxylation of the zeolite is hampered.

The Cu/Al molar ratios of the catalyst series ranged from 0.31 (2 wt% Cu loading) to 0.85 (14 wt% Cu loading). Referring the exchange capacity of the zeolite to Cu^{+}, 31% was achieved at 2 wt% and 85% of the available capacity is consumed at 14% Cu loading.

4.2. Site occupancy

The fact that up to 5 wt% Cu loading on zeolite Y yielded no noteworthy activity seems to contradict proposals that isolated, coordinatively unsaturated Cu ions are the active sites. But the specific site configuration and hence cation distribution within the faujasite structure [31] must be taken into account. Favored sites for fixation of transition metal cations are localized at positions within hexagonal prisms connecting the sodalite units of zeolite Y. Copper ions located at these sites are not accessible for molecules such as CO or N_2 and cannot take part in the carbonylation reaction. Further sites face the supercage and are available for the reaction.

The site capacity of the hexagonal prisms at temperatures above 190 °C amounts to ca. 15 copper cations per unit cell, according to Coughlan and Keane [32], and 15.7 copper cations per unit cell according to Maxwell and de Boer [33]. In both cases, divalent copper is meant and calculation is based on the stoichiometry 1 Cu^{2+}:2 Brønsted acid sites for electroneutrality. Relating 15 copper cations to a unit cell capacity of 58 exchangeable cations, approximately 25% of the exchange capacity was represented by these "hidden" sites.

An estimation based on data in the present work shows that 25% of the exchange capacity of 2.62 mmol g^{-1} corresponded to a Cu loading of 4.1 wt%. The close proximity of this value to the minimum loading of Cu (ca. 5–6 wt%) required to get activity supports the assumption that almost all copper of precursors 2Cu-Y_{400}, 4Cu-Y_{400}, and 6Cu-Y_{400} migrated to sites within the hexagonal prisms of the zeolite structure and were not accessible for reaction at low loading. Thus, first these sites must be saturated before copper is forced to coordinate with Brønsted acid sites within the supercage. This corresponds to the variation of the unit cell parameters with copper loading. Unit cell enlargement was observed as long as preferential location of copper ions takes place at sites located within the restricted environment of the hexagonal prisms, but was insignificantly low as soon as location of copper ions within the supercage continued. The catalysts with copper loading exceeding 6 wt% acquired activity. However, a linear increase of active site concentration with further enhanced loading would imply a linear increase of activity. This obviously was not the case, because the activity (MeOH conversion, STY of DMC; Figs. 11a and 11e) depended exponentially on the copper loading within the range of 6–10 wt% Cu (and even up to 12 wt% Cu if the activation temperature below 750 °C was chosen).

4.3. Mechanism

In 1970, Saegusa et al. [34] reported that the (nonoxidative) reaction of cupric dimethoxide and carbon monoxide in an autoclave led to DMC. The results were explained by the insertion of carbon monoxide into the copper–oxygen bond of cupric dimethoxide to generate carbo-methoxy cupric species, which then underwent coupling with an adjacent methoxyl group. The coupling between the carbomethoxy and methoxyl ligands with release of DMC reduced Cu^{2+} to Cu^{+}. The stoichiometric reaction ran to complete consumption of the methoxide.

For the slurry-phase reaction system with copper chloride, it was suggested [35] that the oxidative carbonylation of MeOH to form DMC proceeds in two steps, with the oxidation of CuCl to $(CH_3O–Cu)^{+}Cl^{-}$ (cupric methoxy-chloride) reduced by CO to DMC in a second step. Because chloride is actually not directly involved, it should be possible to replace chloride by the negatively charged anionic zeolite lattice [6].

King [6] studied the reaction steps (i) methoxide formation, (ii) insertion of CO into methoxide, and (iii) MeOH reaction with carbo-methoxide over Cu/zeolite Y by infrared spectroscopy at 130 °C. He showed that methoxide was formed with copper (the zeolite itself gave no methoxide species), and oxygen promoted formation of Cu-methoxide. Admission of gaseous CO led to carbo-methoxide (with some ambiguities remaining), and further reaction with MeOH/air led to DMC.

Although this investigation was performed for CuCl/zeolite Y, the considerations are valid for Cu_2O/zeolite Y as well, because no interference of Cl in the reaction mechanism was necessary. Catalysts were prepared by mechanical mixing of CuCl or Cu_2O with the zeolite and subsequent heating under flowing helium at 650 °C for 70 h, which is known to lead to a solid-state ion exchange.

The same approach was applied by Anderson and Root [8,9] for preparation of Cu/zeolite X (30% Cu) and Cu/zeolite ZSM-5 (7% Cu). The mechanism involves the adsorption of CO on Cu^{+} but suggests a Rideal–Eley type insertion of CO into surface methoxide directly from the gas phase, because the influence of CO gas-phase pressure was found to be of first order.

All preliminary characterization by DRIFTS measurements [36] confirmed the formation of methoxide as well as the fixation of CO to Cu^{+}, so that the same mechanism probably proceeds. Thus, the high activity achieved through the specific inert activation procedure is associated predominantly with the creation of a favorable active site configuration.

4.4. Comparison of productivity

Comparison of activities is difficult, because catalysts are evaluated mainly in fixed-bed integral-flow reactors for conversion, selectivity, and productivity (STY). Conversion, selectivity, and productivity are largely dependent on the space velocity. High conversion and selectivity at a low space velocity leads to low STY, whereas high STY can be achieved even at low conversion and selectivities if the space velocity is high. For DMC, it has to be differentiated whether selectivity is referred to the conversion of MeOH or to the conversion of CO. In the former case, the stoichiometry has to consider that 2 mol of MeOH are required to produce 1 mol of DMC [Eq. (4)].

The highest values reported in the open literature for a normal-pressure gas-phase oxidative carbonylation of MeOH was given for a $PdCl_2$–$CuCl_2$–CH_3COOK co-impregnated AC catalyst (STY of DMC ca. 390 $g_{DMC}\, l_{Cat}^{-1}\, h^{-1}$) [12]. However, the catalyst suffered considerable deactivation after a process time of 6 h, but still maintained an STY of DMC $> 100\ g_{DMC}\, l_{Cat}^{-1}\, h^{-1}$ with high DMC selectivity (>95%) and MeOH conversions of 3–7% at 130 °C. Values achievable from CuCl/zeolite systems (solid-state ion exchange) were in the range of 40–80 $g_{DMC}\, l_{Cat}^{-1}\, h^{-1}$ [6–9].

The maximum STY of DMC values observed during the present investigation were in the same range, but could be enhanced to nearly 100 $g_{DMC}\, l_{Cat}^{-1}\, h^{-1}$ by operating the sample 12Cu-Y_{700} at slightly higher reaction temperatures (150–160 °C). DMC selectivity was decreased to ca. 45% under these conditions, but the nearly exclusive side product was DMM. For fuel blending, separation of both products is not really necessary, although the O content of DMM is lower than that of DMC. In any case, no chloride impurity needs to be feared.

As will be shown in a forthcoming paper [37] (see additional material), higher DMC selectivities and STY of DMC

are accessible with copper-impregnated zeolite Y under flow conditions at 0.8–1.2 MPa and optimized feed composition allowing an STY of DMC of up to 560 $g_{DMC}\, l_{Cat}^{-1}\, h^{-1}$ at DMC selectivity levels of 70–80%.

5. Conclusion

It has been shown that preparation of Cl-free Cu/zeolite catalysts for the oxidative gas-phase carbonylation of DMC is possible by starting with Cu(II) salts. To obtain noteworthy activity, inert treatment of Cu^{2+}-containing precursors at high temperatures is necessary to allow for autoreduction of Cu^{2+} to Cu^{+}, migration of cations from outer surface areas to the interior, and eventual fixation of Cu^{+} to Brønsted acid sites of the zeolite. Actually, the temperature of inert activation is beyond the upper limit of thermal stability of the zeolite, but is applicable due to the observed stabilizing effect of copper ions. Thus, residual Brønsted acid sites of the zeolite are removed by dehydroxylation, thereby influencing the surface redox properties of Cu^{+}/Cu^{2+} (e.g., facilitating reduction of Cu^{2+} ions). If copper loading and activation temperature are chosen appropriately then the catalyst samples are active for gas-phase carbonylation of MeOH at normal pressure with optimum performance at a loading of 12 wt% Cu, activated at 700–725 °C. STYs of DMC amounted to 100 $g_{DMC}\, l_{Cat}^{-1}\, h^{-1}$ at 150 °C and a GHSV of 3000 h^{-1}.

The catalysts operate without any chloride admixture quite stable. An STY of ca. 60 $g_{DMC}\, l_{Cat}^{-1}\, h^{-1}$ at a reaction temperature of 150 °C could be maintained over 100 h without significant deactivation.

Precipitation allows copper loading up to ca. 14 wt%, because the required high activation temperatures lead to melting of the catalyst in the course of activation, with formation of a glassy amorphous copper aluminate/silicate phase. This is due in part to the enrichment of copper on the outer surface of the zeolite crystallites at higher loadings, where migration and ion exchange become increasingly difficult.

Acknowledgments

Financial support was provided by the Federal Ministry for Education and Research of the FRG, the Senate of Berlin, and the European Union (project 03X2002). The authors thank U. Marx for technical assistance.

Additional material

The online version of this article contains additional material.

Please visit DOI: 10.1016/j.jcat.2006.09.009

References

[1] M.A. Pacheco, Ch.L. Marshall, Energy Fuels 11 (1997) 2.
[2] D. Delledonne, F. Rivetti, U. Romano, Appl. Catal. A Gen. 221 (2001) 241.
[3] P. Tundo, M. Selva, Acc. Chem. Res. 35 (2002) 706.
[4] P. Tundo, Chim. Oggi 22 (2004) 31.
[5] S. Uchiumi, K. Ataka, T. Matsuzaki, J. Organomet. Chem. 576 (1999) 279.
[6] S.T. King, J. Catal. 161 (1996) 530.
[7] S.T. King, Catal. Today 161 (1997) 173.
[8] S.A. Anderson, T.W. Root, J. Catal. 217 (2003) 396.
[9] S.A. Anderson, T.W. Root, J. Molec. Catal. A Chem. 220 (2004) 247.
[10] Y. Cao, J.-Ch. Hu, P. Yang, W.-L. Dai, K.-N. Fan, Chem. Commun. (2003) 908.
[11] I.J. Drake, K.L. Fujdala, A.T. Bell, T.D. Tilley, J. Catal. 229 (2005) 538.
[12] P. Yang, Y. Cao, W.-L. Dai, J.-F. Deng, K.-N. Fan, Appl. Catal. A Gen. 243 (2003) 323.
[13] Atlas of zeolite structures, http://topaz.ethz.ch/IZA-SC/StdAtlas.htm.
[14] R. Szostak, Stud. Surf. Sci. Catal. 58 (1991) 153.
[15] O.P. Tkachenko, K.V. Klementiev, M.W.E. van den Berg, N. Koc, M. Bandyopadhyay, A. Birkner, C. Wöll, H. Gies, W. Grünert, J. Phys. Chem. B 109 (2005) 20979.
[16] R.G. Herman, J.H. Lunsford, H. Beyer, P.A. Jacobs, J.B. Uytterhoeven, J. Phys. Chem. 79 (1975) 2388.
[17] M. Afza, G. Yasmeen, M. Saleem, J. Afzal, J. Therm. Anal. Calorim. 62 (2000) 277.
[18] G.T. Palomino, P. Fisicaro, S. Bordiga, A. Zecchina, E. Giamello, C. Lamberti, J. Phys. Chem. B 104 (2000) 4064.
[19] A. Delabie, K. Pierloot, M.H. Groothaert, R.A. Schoonheydt, L.G. Vanquickenborne, Eur. J. Inorg. Chem. (2002) 515.
[20] K. Matar, D. Goldfarb, J. Phys. Chem. 96 (1992) 3100.
[21] E.F. Vansant, J.H. Lunsford, J. Phys. Chem. 76 (1972) 2860.
[22] J.S. Yu, L. Kevan, J. Phys. Chem. 95 (1991) 6648.
[23] G.T. Palomino, S. Bordiga, A. Zecchina, G.L. Marra, C. Lamberti, J. Phys. Chem. B 104 (2000) 8641.
[24] S.A. Anderson, S. Manthata, Th.W. Root, Appl. Catal. A Gen. 280 (2005) 117.
[25] Y. Fu, T. Hong, J. Chen, A. Auroux, J. Shen, Thermochim. Acta 434 (2005) 22.
[26] R.M. Haniffa, K. Seff, Microporous Mesoporous Mater. 25 (1998) 137.
[27] B. Wichterlová, Z. Sobalík, M. Skokánek, Appl. Catal. A Gen. 103 (1993) 269.
[28] J.W. Ward, J. Catal. 9 (1967) 225.
[29] H.Y. Chen, L. Chen, J. Lin, K.L. Tan, J. Li, Inorg. Chem. 36 (1997) 1417.
[30] J. Sarkany, G.-D. Lei, J.Y. Yan, W.M.H. Sachtler, J. Phys. Chem. 100 (1996) 845.
[31] D. Berthomiéu, J.-M. Ducéré, A. Goursot, J. Phys. Chem. B 106 (2002) 7483.
[32] B. Coughlan, M.A. Keane, J. Chem. Soc. Faraday Trans. 86 (1990) 1007.
[33] I.E. Maxwell, J.J. de Boer, J. Phys. Chem. 79 (1975) 1874.
[34] T. Saegusa, R. Tsuda, K. Isayama, J. Org. Chem. 35 (1970) 2976.
[35] U. Romano, R. Tesel, M.M. Mauri, P. Rebora, Ind. Eng. Chem. Prod. Res. Dev. 19 (1980) 396.
[36] E. Schreier, unpublished results.
[37] M. Richter, M.J.G. Fait, R. Eckelt, E. Schreier, M. Schneider, M.-M. Pohl, R. Fricke, Appl. Catal. B Environ., submitted for publication.